



THE UNIVERSITY *of* EDINBURGH

Edinburgh Research Explorer

Wastewater treatment valorisation by simultaneously removing and recovering phosphate and ammonia from municipal effluents using a mechano-thermo activated magnesite technology

Citation for published version:

Mavhungu, A, Mbaya, R, Masindi, V, Foteinis, S, Muedi, KL, Kortidis, I & Chatzisyneon, E 2019, 'Wastewater treatment valorisation by simultaneously removing and recovering phosphate and ammonia from municipal effluents using a mechano-thermo activated magnesite technology', *Journal of Environmental Management*, vol. 250, 109493. <https://doi.org/10.1016/j.jenvman.2019.109493>

Digital Object Identifier (DOI):

[10.1016/j.jenvman.2019.109493](https://doi.org/10.1016/j.jenvman.2019.109493)

Link:

[Link to publication record in Edinburgh Research Explorer](#)

Document Version:

Peer reviewed version

Published In:

Journal of Environmental Management

General rights

Copyright for the publications made accessible via the Edinburgh Research Explorer is retained by the author(s) and / or other copyright owners and it is a condition of accessing these publications that users recognise and abide by the legal requirements associated with these rights.

Take down policy

The University of Edinburgh has made every reasonable effort to ensure that Edinburgh Research Explorer content complies with UK legislation. If you believe that the public display of this file breaches copyright please contact openaccess@ed.ac.uk providing details, and we will remove access to the work immediately and investigate your claim.



Wastewater treatment valorisation by simultaneously removing and recovering phosphate and ammonia from municipal effluents using a mechano-thermo activated magnesite technology

A. Mavhungu¹, R. Mbaya¹, V. Masindi^{2&3}, S. Foteinis^{2*}, K.L. Muedi², I. Kortidis⁴ and E. Chatzisyneon⁵

¹Department of Chemical, Metallurgy and Materials Engineering, Staatsartillerie Rd, Pretoria West 0183, Tshwane, University of Technology, Pretoria, South Africa

²Council for Scientific and Industrial Research (CSIR), Built Environment (BE), Hydraulic Infrastructure Engineering (HIE), P.O Box 395, Pretoria, 0001, South Africa, Tel: +2712 841 4107, Fax: +27128414847, VMasindi@csir.co.za, masindivhahangwele@gmail.com

³Department of Environmental Sciences, School of Agriculture and Environmental Sciences, University of South Africa (UNISA), P. O. Box 392, Florida, 1710, South Africa

⁴Department of Physics and Engineering, University of Zululand, Kwadlangezwa, 3886, South Africa

⁵School of Engineering, Institute for Infrastructure and Environment, University of Edinburgh, Edinburgh EH9 3JL, United Kingdom

Abstract

Phosphate and nitrate enrichment largely impair aquatic ecosystem functions and services, thus comprising an emerging problem of environmental concern. The problem pertains to developing countries where phosphate and nitrate discharge to surface water is on the rise due to a rapid growth in population. Herein, these pollutants (phosphate and ammonia) were removed from real municipal wastewater using a simple, fast, and cost-effective process. Raw cryptocrystalline magnesite, a mineral abundant in South Africa, was simply milled and calcined (mechano-thermo processing) in order to produce the activated magnesite (feed). The feed was then used in batch processing for pollutants adsorption and precipitation from real wastewater. The process was optimised by varying the treatment or contact time, feed dosage, concentration, pH, and temperature. The feed and product mineral (produced sludge) were characterised using X-ray Diffraction (XRD), field emission scanning electron microscopy (FESEM) compatible with energy dispersive spectroscopy (EDS), and Fourier Transform Infrared Spectrometer (FTIR). It was identified that the optimal conditions differed for each pollutant, highlighting the importance of tailoring the process to fit the local wastewater characteristics and as part of a treatment train system. Specifically, maximum P removal was achieved after 5 min of mixing, using 1 g L⁻¹ of feed, 123 mg L⁻¹ initial phosphate concentration, pH 8 – 10, and was not affected by temperature variations; whereas, for ammonia removal, optimal conditions were 180 min, 16 g L⁻¹ feed dosage, 80 mg L⁻¹ initial concentration, pH 10 and temperature > 45 °C. The optimal conditions for the removal of both pollutants from real wastewater were 30 min, 8 g L⁻¹ dosage, 7.5 pH, 35 °C. Furthermore, Mg and Ca concentration was found to influence the process. Reduction in total dissolved solids and electrical conductivity suggest an attenuation of chemical species. Characterisation revealed that the product mineral obtained under the optimal conditions for pollutants removal is rich in quartz, periclase, brucite, calcite, magnesite, and struvite. This was further supported by the FTIR results, which indicated the presence of Mg-O, PO₄³⁻, N-H and -OH stretches. In addition, the EDS verified the presence of Mg, Ca and P in product mineral. Results are suggestive of the high efficiency of the mechano-thermo activated magnesite treatment process for P and N removal and struvite crystallization. Thus, this technology could valorise municipal wastewater effluents and open new horizons for the

*Corresponding author: sfoteinis@gmail.com

48 effective and sustainable management of wastewater effluents, since struvite can replace the
49 mined phosphate fertilizers, which are rapidly depleting, in the agriculture industry.

50 **Keywords:** Mechano-thermo treatment; Pre-treated magnesite; Phosphorus; Nitrogen;
51 municipal effluents; magnesium ammonium phosphate (struvite), sustainable

52

53 **1 Introduction**

54 Nowadays, research has focused on identifying feasible and practical approaches to manage
55 high levels of phosphate and ammonia contained in wastewater streams, especially in
56 developing countries where wastewater could be poorly treated. A wide range of
57 technologies, based on different techniques and mechanisms, have been developed and
58 explored, with biological processes, adsorption, filtration, bio-sorption, phytoremediation and
59 crystallisation being popular for phosphate and ammonia removal from wastewater (Li et al.,
60 2017; Peng et al., 2018; Satoshi et al., 2013). Adsorption has been used to remove phosphate
61 and ammonia from wastewater, typically at bench and semi-industrial scale using clay
62 minerals, metals and their composites, while filtration techniques have been explored as well
63 (Goh et al., 2008; Huang et al., 2017; Satoshi et al., 2013; Yagi and Fukushi, 2012; Zulfiqar
64 et al., 2014). Adsorption followed by crystals settling is particularly popular (Li et al., 2015;
65 Li et al., 2017), with Ca^{2+} or Mg^{2+} based materials being typically used as precursors (Li et
66 al., 2017; Peng et al., 2018; Stolzenburg et al., 2015). Other adsorbents include elements that
67 have high affinity to phosphate and ammonia, mainly trivalent metals, such as Fe^{3+} and Al^{3+} ,
68 which have the added benefit of regeneration (Benyoucef and Amrani, 2012; Chiban et al.,
69 2012; Deng et al., 2016; Egle et al., 2016; Gao et al., 2018; Goh et al., 2008).

70 South Africa is well-endowed with cryptocrystalline magnesite, which makes it a perfect
71 candidate material for sustainable wastewater treatment and phosphate and ammonia removal
72 (Magagane et al., 2019). This material is rich in Mg and it is well established that treating
73 wastewater with Mg^{2+} based minerals can result to the formation of magnesium ammonium
74 phosphate (struvite), which has a number of industrial applications (Bayuseno and Schmahl,
75 2018; Kozik et al., 2014; Stolzenburg et al., 2015; Sutyono et al., 2016; Wang et al., 2017);
76 albeit its production depends on a number of factors such as treatment or contact time,
77 dosage, pH, and temperature (Li et al., 2017). A number of salts that bear Mg^{2+} ions have
78 been used for struvite crystallisation, including MgCl_2 , $\text{Mg}(\text{OH})_2$ and MgO (Peng et al.,
79 2018; Stolzenburg et al., 2015; Wang et al., 2017); however, these are mainly commercially

80 available salts, typically associated with high manufacturing costs which hinders the
81 commercial application of the process (Muhmood et al., 2019).

82 For the case of South Africa, a developing country, a low cost and easily accessible
83 replacement Mg source is required to make the process commercially attractive. Due to its
84 high Mg content, amorphous and cryptocrystalline magnesite could be a possible source of
85 Mg^{2+} and Ca^{2+} for the removal of phosphate and ammonia from aqueous matrices. These
86 materials have been explored for mine water treatment and the management of other
87 contaminants (Masindi, 2017; Masindi et al., 2016a; Masindi et al., 2018a; Masindi et al.,
88 2018b; Masindi et al., 2016b). Specifically, Masindi et al. (2016a) highlighted that
89 cryptocrystalline magnesite, and its pre-treated derivative (Magagane et al., 2019), are
90 characterised of Mg, Ca, Fe and Si sandwiched together, hence giving it an up-hand due to
91 hybrid properties therein. The mineral phases can also aid in the removal of phosphate and
92 ammonia from wastewater, eventually leading to the formation of struvite. It should be noted
93 that the precipitation of struvite from wastewater streams is gaining the attention of the
94 scientific community due to its potential for phosphorus recovering for fertilization (Yan and
95 Shih, 2016), and particularly owing to the fact that phosphate rock, a non-renewable resource,
96 is predicted to be depleted within the next 100 years (Li et al., 2019). Furthermore, apart from
97 calcium and magnesium, (Torzewska and Róźalski, 2015) noted that certain bacteria, such as
98 the genus *Proteus*, can also play a role in inducing struvite crystallization. (Wąsik et al.,
99 2017) also noted that coliform bacteria, in the presence of magnesium and calcium ions,
100 among others, can create suitable conditions for the formation of struvite crystals. (Yan and
101 Shih, 2016) studied the effects of calcium and ferric ions on struvite precipitation, while (Liu
102 and Wang, 2019) noted that wastewater with the Ca/Mg ratio above 1/2 is not suitable for
103 phosphorus recovery, due to the low proportion of struvite recovery. Finally, Li et al. (2019)
104 reviewed the key aspects for struvite process design and development, the research trends,
105 product application and process economics.

106 Herein, based on preliminary results of our group (Mavhungu et al., 2018), we
107 comprehensively examine the feasibility of South African pre-treated magnesite, rather than
108 commercial salts, for phosphate and ammonia removal from real wastewater. This study also
109 sheds light on the mechanisms governing the removal of pollutants from aquatic matrices
110 through struvite precipitation. Furthermore, struvite, a process co-product, has an economic
111 value, since if recovered could be suitable for reuse in agriculture (Taddeo et al., 2018).

112 Therefore, its recovery could both reduce the cost and environmental impact of the
113 wastewater treatment process, which will be examined in future works of our group.

114

115 **2 Materials and methods**

116 **2.1 Wastewater and raw cryptocrystalline magnesite collection**

117 Real untreated wastewater, rich in phosphate and ammonia, was collected from a municipal
118 wastewater treatment facility in Pretoria, South Africa. The treatment facility receives
119 wastewater from a number of activities from the surrounding area. High-density polyethylene
120 (HDPE) wide-mouth bottles were used for sample collection. Solids and debris were removed
121 by filtration, using Macherey-Nagel filter papers (MN 615. Ø125mm), and the samples were
122 used immediately thereafter. In the context of this work, the wastewater was diluted, as
123 required, to reach the desired phosphate and ammonia concentration. Raw cryptocrystalline
124 magnesite samples were collected from an abandoned magnesite mine in Folovhodwe,
125 Limpopo Province, South Africa.

126 **2.2 Production of the mechano-thermo activated magnesite**

127 The collected raw cryptocrystalline magnesite was first milled into a fine powder, using a
128 vibratory ball miller at 500 rpm for 15 min. Thence, the fine powder was calcined at 1,000
129 °C, using a furnace as reported in our previous study (Magagane et al., 2019). Finally, the
130 samples were milled again, under the same conditions, and then sieved through 32 microns
131 perforated sieve. The thermo-mechano (i.e. calcined and milled) activated magnesite samples,
132 feed thereafter, were then stored in zip-lock plastic bags until utilisation for simultaneous
133 adsorption of phosphate and ammonia.

134 **2.3 Quality control and quality assurance**

135 Experiments were performed in triplicate, giving similar results, and are reported as mean
136 average values. For quality control and assurance, ISO-accredited laboratories and NIST
137 standards were used for sample analyses. To ensure reliable, accurate, and high precision
138 results inter-laboratory analysis was also undertaken, i.e. for validation and verification
139 purposes.

140 **2.4 Process optimisation**

141 For process optimization and to obtain an in-depth understanding of the factors influencing
 142 phosphate and ammonia removal, a number of operational parameters were evaluated. These
 143 include: i) contact time (i.e. mixing duration of the feed-wastewater solution); ii) feed dosage
 144 (i.e. the amount of mechano-thermo activated magnesite used during treatment); iii) chemical
 145 species concentration (i.e. phosphate and ammonia initial concentration); iv) pH; and v)
 146 temperature. Experiments were performed in 500 mL volumetric flasks (low-form beaker),
 147 stirred at 500 rpm using an overhead stirrer. To gain insight, the one-factor-at-a-time (OFAT)
 148 method was used, i.e. each time one parameter was varied while the others were fixed, as
 149 shown in Table 1.

150 **Table 1:** Process parameters assayed for the optimisation of phosphate and ammonia removal
 151 from wastewater.

Parameter	Units	Data variation range
Contact time	minutes (min)	1; 5; 10; 30; 60; 120; 150; 180; 240; and 300
Dosage	grams*	0.1; 0.5; 1; 2; 3; 4; 5; 8; and 10
Concentration	mg L ⁻¹ or ppm	2; 4; 8; 12; 16; 21; 33; 41; 82; and 123
pH of solution	N/A	1, 2, 3, 4, 5, 6, 7, 8, 9, 10, 11, and 12
Temperature	°C	35; 45; 55; 65; and 75

*per 500 mL of wastewater

152

153 The effect of the initial phosphate and ammonia concentration was studied by diluting the
 154 raw municipal wastewater to the desired concentration (Table 1). The pH was adjusted using
 155 0.1 M NaOH and/or 0.1 M HCl, as required. A 4-decimal place analytical balance was used
 156 to calculate feed dosages. Finally, the temperature was regulated using a hotplate stirrer and
 157 the effect of contact time was examined by agitating the wastewater-feed solution at the time
 158 intervals specified in Table 1.

159 2.5 Percentage removal

160 The amount of phosphate and ammonia removed from municipal wastewater was estimated
 161 using equation (1), i.e.:

$$162 \quad \% \text{ Removal} = \frac{C_0 - C_e}{C_0} \times 100 \quad (1)$$

163 where C_0 is the initial phosphate or ammonia concentration and C_e is the final concentration,
 164 after treatment, of phosphate or ammonia.

165 **2.6 Analytical techniques**

166 The pH, Electrical conductivity (EC) and Total Dissolved Solids (TDS) were monitored
 167 using a multi-parameter probe (HANNA instrument, HI9828). Chemical species
 168 concentrations were determined by means of inductively coupled plasma mass spectrometry
 169 (ICP-MS) (7500ce, Agilent, Alpharetta, GA, USA). The raw magnesite, the feed (mechano-
 170 thermo activated magnesite) and product mineral (i.e. the produced sludge that contains
 171 struvite) properties were examined by the analytical techniques detailed in Table 2.

172 **Table 2:** The equipment used for characterisation of feed and product mineral.

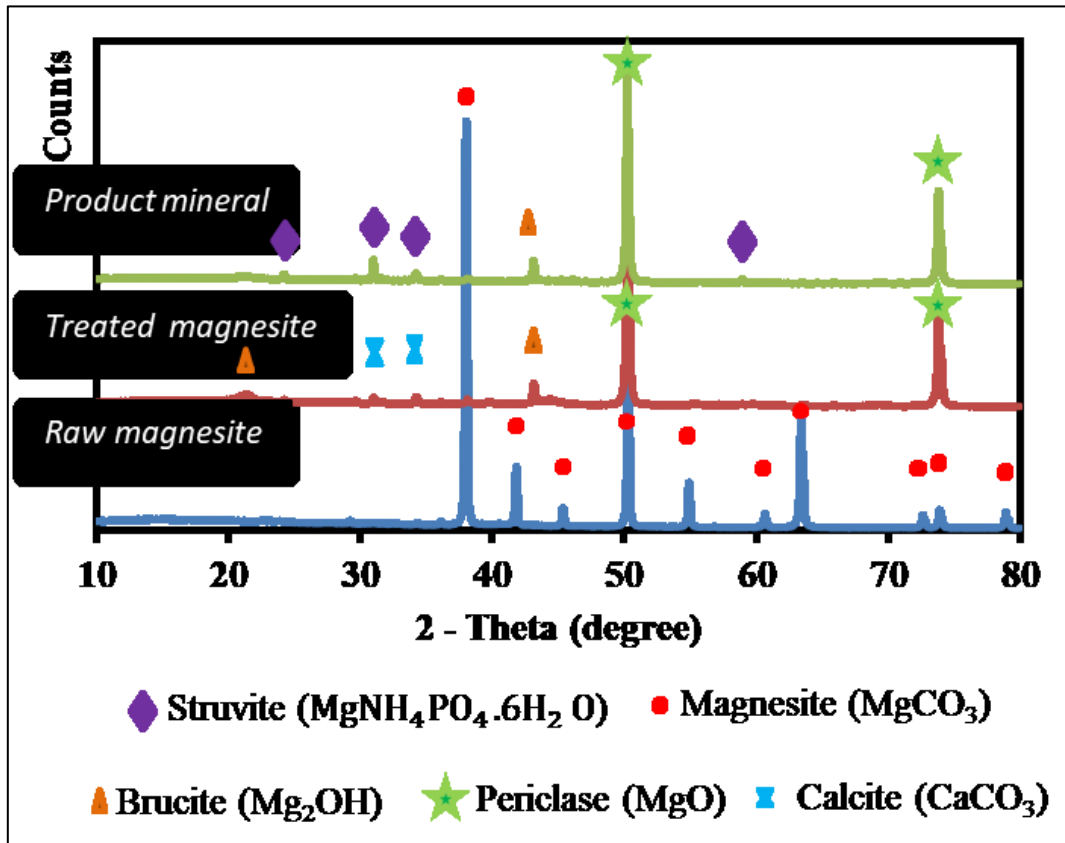
Parameter	Analytical Technique	Model
Mineralogical properties	X-ray Diffraction (XRD)	PANalytical X'Pert PRO-diffractometer equipped with Philips PW 1710 Diffractometer with graphite secondary monochromatic source
Functional groups	Fourier Transform Infrared Spectrometer (FTIR)	Perkin-Elmer Spectrum 100 Fourier Transform Infrared Spectrometer (FTIR) equipped with Perkin-Elmer Precisely Universal Attenuated Total Reflectance (ATR) sampling accessory with a diamond crystal.
Morphology, Mapping and elements	Field Emission Scanning Electron Microscope (FESEM) equipped with Energy-dispersive X-ray spectroscopy (EDS)	Auriga Cobra FIB-FESEM, Carl Zeiss FE-SEM, Germany

173 **3 Results and discussions**

174 **3.1 Characterisation of the raw magnesite, feed, and product mineral**

175 **3.1.1 Mineralogical analysis**

176 The mineralogical properties of the raw magnesite, the feed (mechano-thermo activated
 177 magnesite) and product mineral (produced sludge) were estimated by means of X-ray
 178 Diffraction (XRD) and are shown in Figure 1.



179

180 **Figure 1:** The mineralogical properties of raw magnesite, feed, and product mineral.

181 As shown in Figure 1 there is a change in mineral phases after calcination. Initially, it was
 182 observed that the raw magnesite contains pure magnesium carbonate. However, after
 183 calcination, new phases were observed in the feed and these include periclase, brucite, and
 184 calcite, in addition to amorphous fractions. Finally, the produced sludge (product mineral)
 185 was found to contain struvite, periclase, and brucite. This is an indication that phosphate and
 186 ammonia are adsorbed by the feed and form struvite, as denoted in equation (2):



188 Similar results were reported by Sutyono et al. (2016). Furthermore, the obtained peaks at
 189 21, 23, 31, and 34 2theta degrees are in good agreement with those reported by Li et al.
 190 (2017) and Gao et al. (2018). This confirms that the reaction between the feed and the
 191 wastewater leads to the formation of magnesium ammonium phosphate (struvite). It should

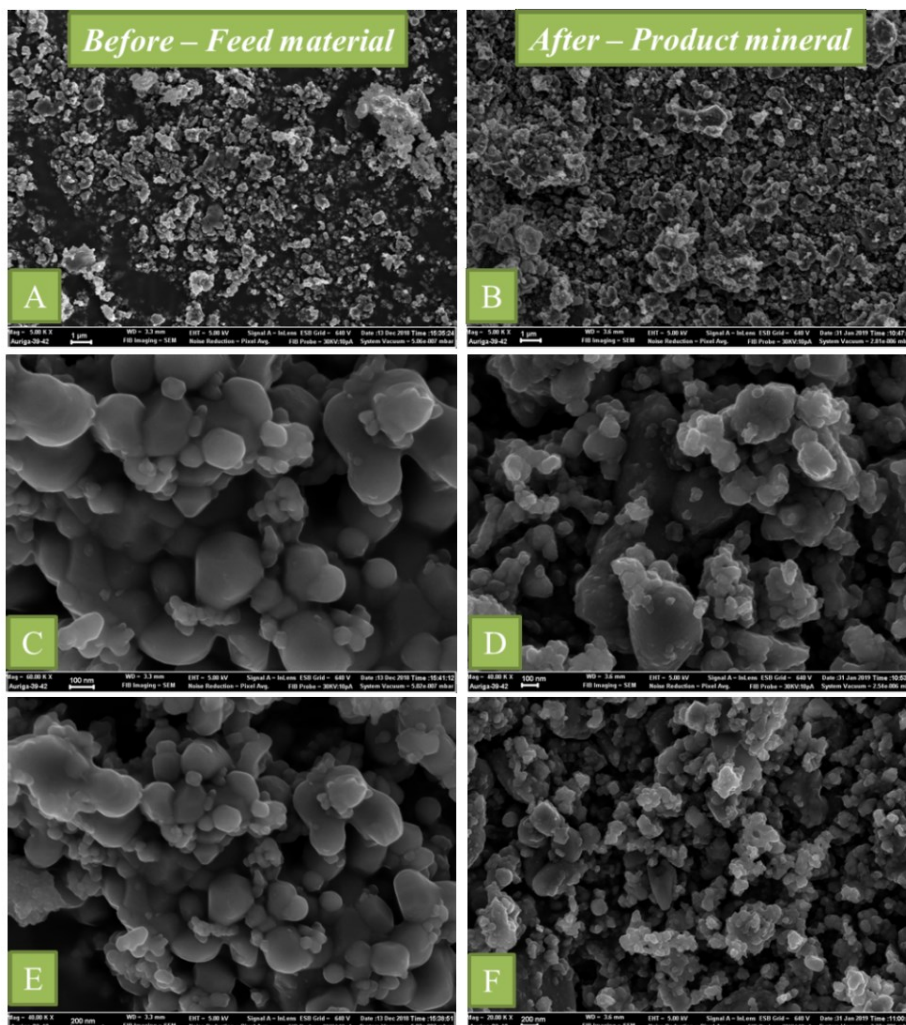
192 be noted that since the activated magnesite (feed) reacts with the wastewater to produce
 193 struvite, it cannot be regenerated or recycled in the process. The other components observed,
 194 such as the periclase and brucite, could be also beneficial since it is envisaged that the
 195 product mineral (struvite) would be used for agriculture purposes. Finally, the presence of
 196 Mg and Ca in the feed contributes towards increasing the pH value of the wastewater and
 197 generating Mg^{2+} and Ca^{2+} . This is shown in eq. (3) – (4):



200 Mg^{2+} will then scavenge the NH_4^+ and PO_4^{3-} to form a complex, as denoted in equation 2.

201 **3.1.2 Morphological properties**

202 The morphological properties of the feed and product mineral were measured by a Field
 203 Emission Scanning Electron Microscope (FESEM). The clear, ultra-high resolution and low
 204 electrostatically distorted images obtained by the FESEM are shown in Figure 2.



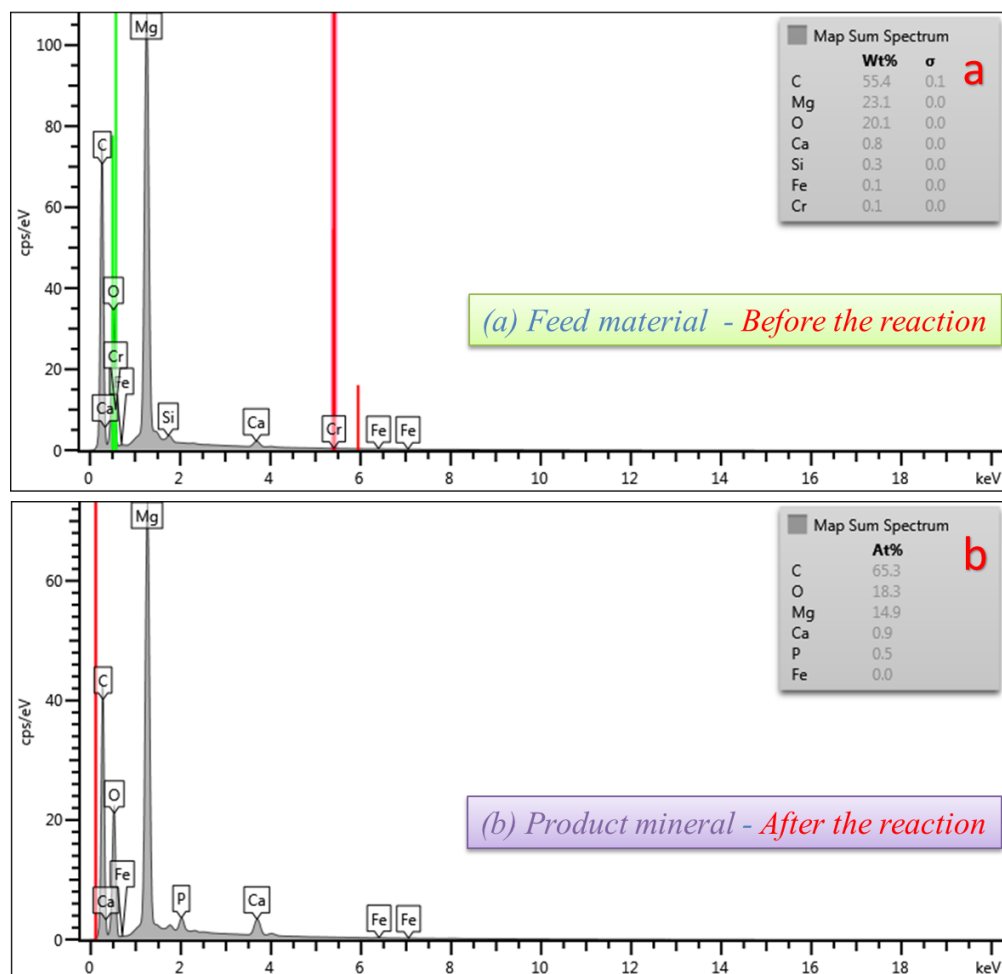
205

206 **Figure 2:** The morphological properties of the feed (left-hand-side) and product mineral
 207 (right-hand-side) obtained by FESEM at 1 μm (A and B), 100 nm (C and D), and 200 nm (E
 208 and F).

209 From the comparative analysis between the feed's and the product mineral's morphological
 210 properties shown in Figure 2, it is evident that the feed contains nano-sheets, with hexagonal
 211 structures uniformly distributed across the surface. Contrary, the product mineral portrayed
 212 nanosheet-like structures with reduced size. Therefore, the results are suggestive of a possible
 213 dissolution of the feed material or, more likely, the formation of new mineral phases, as will
 214 be discussed further down. These results are also consistent with those reported by Herald et
 215 al. (2017).

216 3.1.3 Elemental composition of feed and product mineral

217 As mentioned above, the FESEM was equipped with an Energy-dispersive X-ray
 218 spectroscopy (EDS) detector, which was used towards identifying the elemental composition
 219 of the feed and of the product mineral.



220

221 **Figure 3:** Elemental composition of the: (a) feed and (b) product mineral.

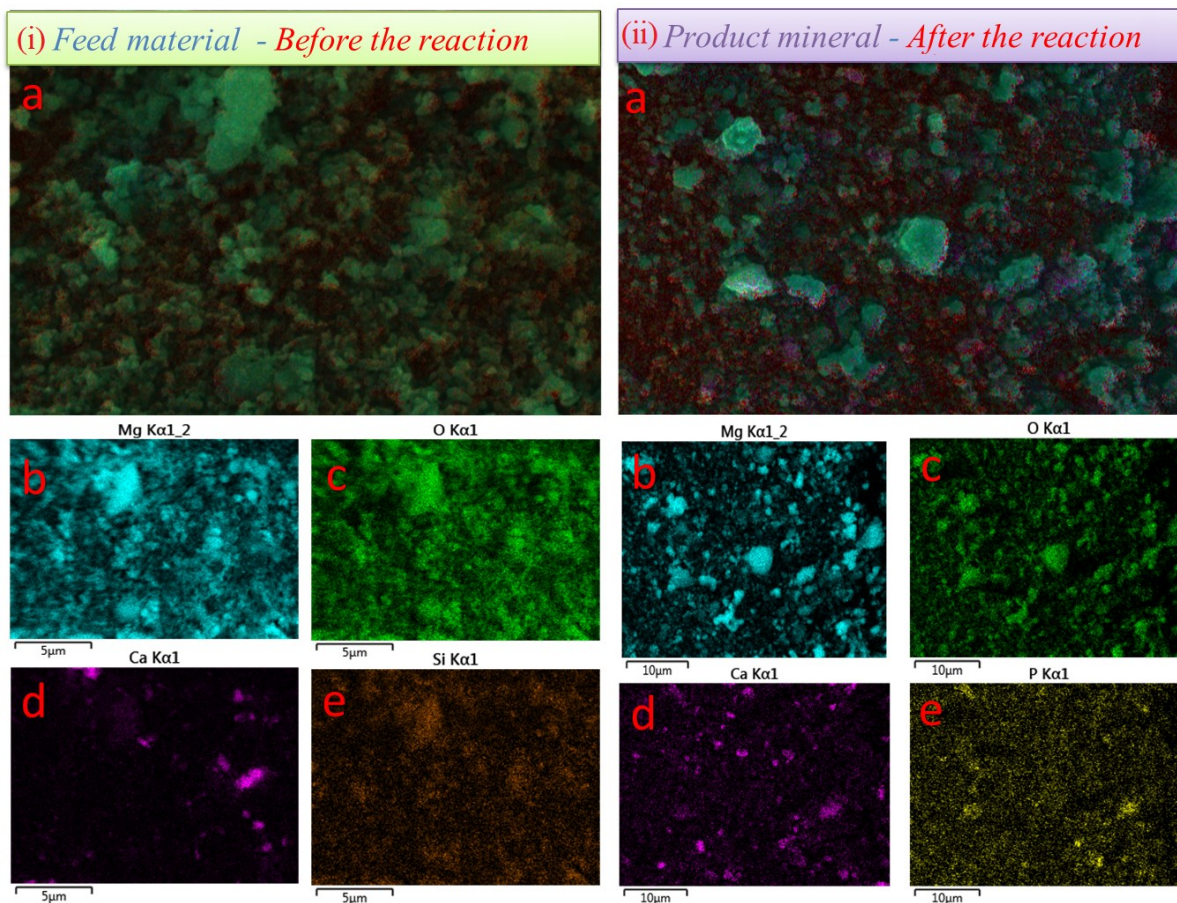
222 Specifically, the feed material (mechano-thermo activated magnesite) was found to contain
223 Mg, O, and C, in addition to traces of Ca, and Si (Figure 3). This composition will
224 accommodate an increase in the pH of the wastewater-feed mixture. Furthermore, as
225 discussed above, Mg contributes to the removal of NH_4^+ and PO_4^{3-} from wastewater, which is
226 the main target of this work. Finally, the product mineral (Figure 3b) contains Mg, O, and C,
227 as major components, while traces of Ca and P were also observed. This, along with the
228 observed water quality of the treated water (Table B1 Appendix), suggests that P has been
229 removed from wastewater and fixed in the product mineral (sludge).

230 **3.1.4 Elemental composition analysis**

231 Here the FESEM and the corresponding EDS elemental mapping images for the feed and
232 product mineral are given and discussed, as to gain an in-depth understanding and verify or
233 refute the elemental composition obtained by the EDS element analysis. Specifically, EDS
234 element analysis revealed the existence of Mg, O, Ca, and Si, in the feed and Mg, O, K, P, in
235 the product mineral and therefore FESEM-EDS elemental mapping will focus on them. In
236 Figure 4i the FESEM-EDS layered images of the feed material and for Mg, O, Ca, and Si are
237 shown.

238 The elemental mapping confirmed the existence of Mg, O, Ca, and Si in the feed, which was
239 identified in the elemental composition of feed and product mineral section. These elements
240 contribute to the removal of phosphate and ammonia from wastewater, while both Mg and Ca
241 contribute to an increase of the pH, as discussed in the mineralogical analysis section.
242 Furthermore, the identified elemental composition of product mineral was also confirmed by
243 the FESEM-EDS imagery, as shown in Figure 4ii. Specifically, the elemental mapping of the
244 product mineral revealed that indeed the product mineral contains Mg, O, Ca and P, as shown
245 in Figure 4ii (b), (c), (d), and (e), respectively. This is an indication that Si was released as
246 the pH was increasing and Mg, Ca and P formed struvite, hence achieving a high removal
247 capacity as will be discussed further down.

248

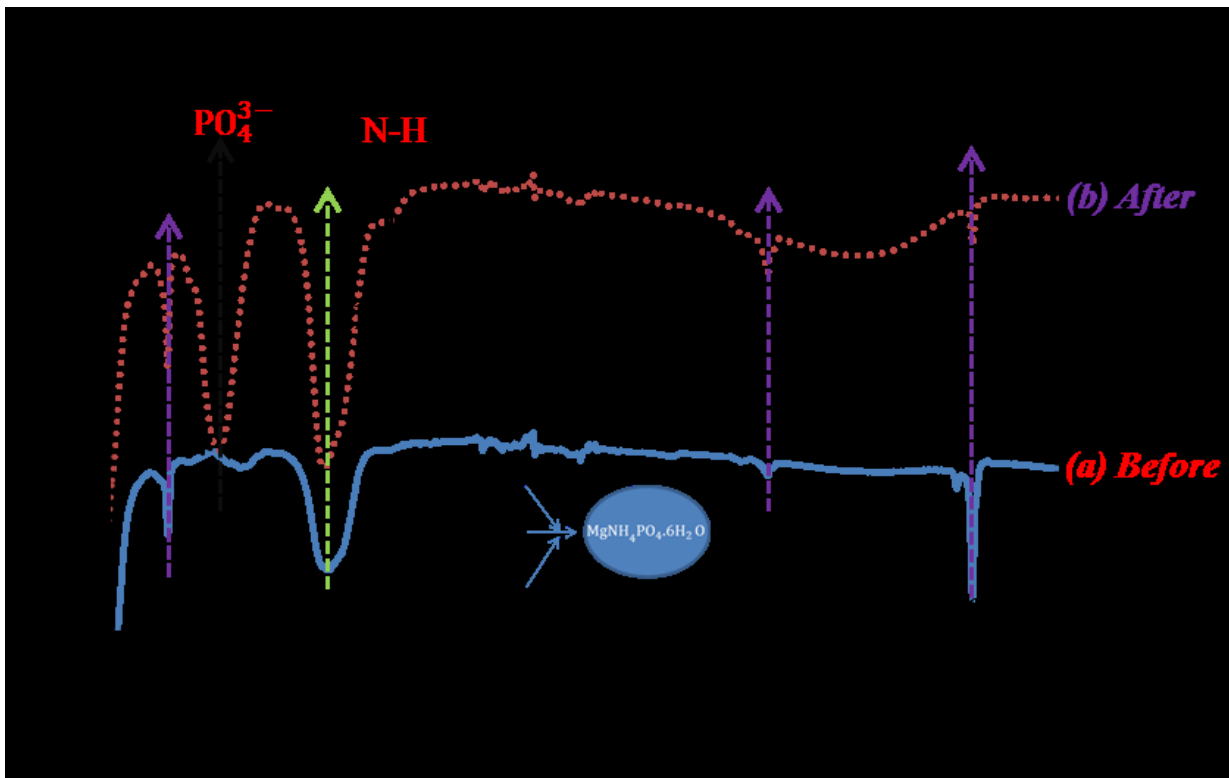


249

250 **Figure 4:** (i) The FESEM image of the: (a) feed material and the FESEM-EDS layered
 251 images of the feed material for: (b) Mg, (c) O, (d) Ca, and (e) Si; and (ii) the FESEM image
 252 for the: (a) product mineral, and the FESEM-EDS layered images of the feed material for (b)
 253 Mg, (c) O, (d) Ca, and (e) P.

254 3.1.5 Fourier transform infrared spectroscopy analysis

255 The results of the Fourier transform infrared spectroscopy (FTIR) analysis, both for the feed
 256 and the product mineral are shown in Figure 5. Furthermore, the identified functional groups
 257 and wavenumber of feed and product mineral are given.



258

259 **Figure 5:** The FTIR results for the feed and product mineral.

260 The wavenumbers of the peaks of the feed and the product mineral (Figure 5) were compared
 261 with those obtained from the literature (Herald et al., 2017; Magagane et al., 2019) and were
 262 found to be in good agreement. Furthermore, the FTIR spectrum of the feed confirms the
 263 existence of water hydration, Mg-O metal-oxygen bond, and carbonate. This corroborates the
 264 XRD results and is an indication of the presence of periclase and traces of brucite in the feed.
 265 Furthermore, in the FTIR spectrum of the feed, the presence of carbonate was identified,
 266 which was expected since it is a residue of the calcination process. Finally, the FTIR
 267 spectrum of the product mineral was observed to contain water hydration, Mg-O metal-
 268 oxygen bond, N-H bond, and PO_4^{3-} , hence confirming that struvite has been formed. Overall,
 269 the obtained results are in agreement with those reported in the literature (Herald et al.,
 270 2017) and further support the results obtained by the EDS and XRD analyses.

271 3.2 Operational parameters optimisation

272 3.2.1 Variation of pollutants removal as a function of contact time

273 First the effect of contact time, i.e. mixing duration, on total dissolved solids (TDS) removal
 274 was examined and then on phosphate and ammonia removal. As mentioned in Table 1a wide
 275 spectrum of mixing durations, i.e. 1, 5, 10, 30, 60, 120, 150, 180, 240, and 300 min, was

276 considered. A sharp decrease in the TDS level/concentration was observed from 0 to 5 min
277 (Figure A1, in the appendix). Thereafter, only trivial fluctuations were observed with
278 increasing contact time. This is a good indication that, in terms of TDS removal, the system
279 reaches equilibrium within the first 5 min of contact time.

280 Moreover, the percentage removal of the targeted pollutants under study, i.e. phosphate and
281 ammonia, along with the measured level of calcium and magnesium, are shown in Figure A2
282 in the appendix, and for the abovementioned contact times. A steep increase in the percentage
283 removal of ammonia was observed during the first 10 min (~68 % removal). Then a decrease
284 in the percentage removal is observed up to the contact time 120 min and thereafter the
285 ammonia percentage removal increases up to the 300 min contact time (~76 % removal).
286 Overall, it can be claimed that the optimal contact time is 180 min, where around 75 % of
287 ammonia is removed, since thereafter ammonia is removed commenced to stabilize, hence
288 suggesting that the reaction has reached equilibrium. On the other hand, the system is highly
289 efficient at removing phosphate, since starting at 1 min, the phosphate removal is ~95 % and
290 then maximized at 5 min (~98 %). Thereafter, it remained constant, with more than 98 % of
291 phosphate being removed. This suggests that the system has reach equilibrium in phosphate
292 removal at 5 min contact time. The abovementioned percentage removals are attributed to the
293 reaction of the feed with phosphate and ammonia. A similar trend has been reported by Yagi
294 and Fukushi (2012).

295 Furthermore, the level of magnesium was observed to follow a somewhat similar pattern with
296 the one observed in ammonia percentage removal, with a step increase in its concentration
297 during the first 30 min, then a decrease at contact time 60 min, then an increase at contact
298 time 90 min and thereafter it remains practically stable (Figure A2 in the appendix). On the
299 other hand, the level of calcium increases at contact time 5 min, then it decreases and
300 thereafter trivial fluctuations are observed.

301 The above indicate that the reaction of Mg^{2+} , Ca^{2+} , NH_4^+ , and PO_4^{3-} (see eq. 2) is leading to
302 the formation of struvite. To afford the reaction adequate time, 5 min was taken as the
303 optimum contact time for the removal of phosphate (more than 98 % is removed) and 180
304 min was taken as the optimum time for the removal of ammonia (around 75 % of the
305 ammonia content is removed). Furthermore, 5 min was considered as the ideal time for the
306 synthesis of struvite using the mechano-thermo treated magnesite. Thus, this study attained a
307 fast struvite formation time, compared to other studies in literature (Sutiyono et al., 2016).

308

3.2.2 Variation of pollutants removal as a function of feed dosage

In this section the effect of feed dosage on TDS removal and on the removal of the targeted pollutants was examined by varying both the feed dosage (from 0.1 to 10 g). Three different contact times were examined, i.e. 10, 30, and 60 min, while the pollutants' initial concentration (contact time 0 min) was also measured.

Regarding TDS removal, it was found that its level/concentration is directly affected by the contact time and feed dosage (Figure A3, appendix). It appears that with increasing mixing time and dosage, TDS concentration decreases. Specifically, apart from the value for the 30 min contact time and dosage 1 g per 500 ml (i.e. 2 g L⁻¹) and the value for the 60 min contact time and dosage 5 g, where a small increase in the TDS level is observed compared to the previously measured value (see Figure A3, appendix), the pattern that was observed was that regardless of the contact time the TDS level decreases with increasing feed dosage, until it is practically near-zero. To be more specific, for contact time 10, 30, and 60 min the TDS is practically near-zero (less than 5 mg L⁻¹) when the dosage is equal or higher than 8 g, 3 g, and 8 g, respectively. Therefore, 30 min and 3 g (i.e. 6 g L⁻¹) were observed to be the most efficient range for the reduction of TDS (Figure A3, appendix).

Furthermore, the effectiveness of the process in removing the targeted pollutants was examined by correlating their percentage removal with varying feed dosages, as described in Table 1. The calcium and magnesium levels were also measured at 30 min contact time and for the examined feed dosages. It was observed that the process is very efficient in phosphate removal (percentage removal > 95 %) even at the lowest dosage, i.e. 0.1 g. For the 0.5 g feed dosage phosphate is practically removed (> 98.3 %) and thereafter remains constant (Figure A4, appendix). This indicates the high affinity of the feed material to phosphate and suggests that the system can operate efficiently even at very low feed dosages. For ammonia removal, a different pattern was observed. The system presents a steep increase in the percentage of ammonia removal from the 0.1 to 0.5 g feed dosage, thence the percentage removal decreases up to 5 g dosage, while a sharp increase in ammonia removal is observed for higher values. The fluctuations in ammonia removal could be explained by the competition to reactive sites.

At the same time, it is observed that the Ca level remained practically constant up to the 4 g feed dosage and thereafter it sharply increase with increasing feed dosage values. On the other hand, the Mg level is observed to decrease up until the 4 g feed dosage, with a sharp decrease observed between 3 g and 4 g, while for 4 g dosage values and higher the Mg level

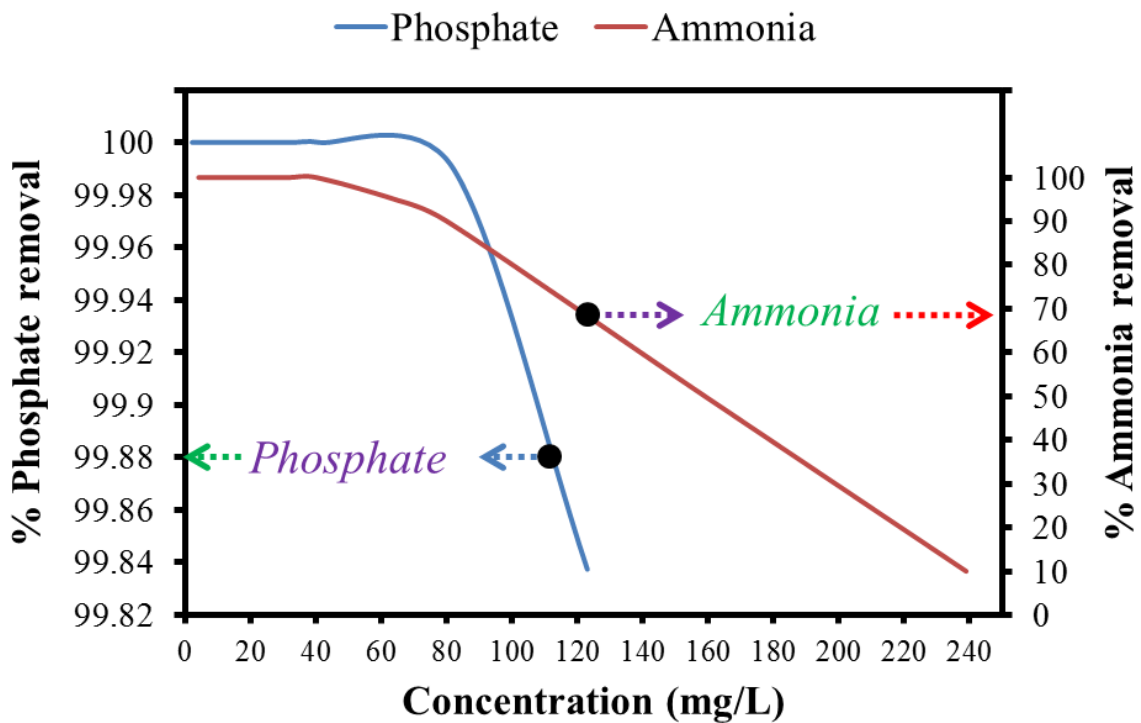
341 is minuscule. This large reduction in the Mg level could be attributed to the increase in pH,
342 traced back to increasing Ca concentration as discussed above, leading to the formation and
343 precipitation of brucite. After the 4 g dosage, the Ca levels were observed to steeply increase
344 with an increase in dosage. This could be attributed to possible dissolution of Ca and Mg
345 from the feed into the wastewater and could be precursors for struvite synthesis.

346 In light of the obtained results, it is concluded that with 0.5 g (i.e. 1 g L⁻¹) dosage phosphate
347 removal is optimized, whereas for ammonia removal optimisation 8 g (i.e. 16 g L⁻¹) dosage is
348 required. Results suggest the importance of tailoring the process parameters according to the
349 characteristics and treatment quality requirements of the targeted wastewater effluent. Here, 3
350 g (i.e. 6 g L⁻¹) was considered as the optimum dosage for the removal of both phosphate and
351 ammonia.

352 **3.2.3 Pollutant removal as a function of their initial concentration**

353 First, the effect of phosphate initial concentration on TDS removal was examined by varying
354 its initial concentration from 2 to 123 mg L⁻¹, as described in Table 1. An increase in TDS
355 removal is observed with increasing initial phosphate concentration, while pH was observed
356 to decrease and particularly a steep decrease is observed for phosphate values higher than 33
357 mg L⁻¹ (Figure A5, appendix). The high pH values observed with low phosphate
358 concentration indicate the over-saturation of the system, with alkaline generating materials
359 (MgO and CaO) elevating the pH. As the phosphate concentration increases, more chemical
360 components are present in the system, which then react with the feed's dissolved chemical
361 components, hence a reduction in pH is observed. As a result, for initial phosphate
362 concentrations between 2 to 21 mg L⁻¹, the TDS level of the system (wastewater-feed) was
363 higher than the initial TDS of the wastewater (Figure A5, appendix), however, in inverse
364 proportion, i.e. as the initial phosphate concentration, and by extension the TDS level of the
365 wastewater, was increasing (up to 33 mg L⁻¹ phosphate concentration) the TDS level of the
366 system was decreasing. This is an indication that the feed addition is increasing the TDS
367 concentration due to the dissolution of chemical components in its matrices. Nevertheless, for
368 phosphate initial concentration higher than 33 mg L⁻¹, and up to 123 mg L⁻¹, the TDS levels
369 of the system were constantly lower than the initial TDS of the wastewater, in direct
370 proportion, which indicate pollutants removal from the wastewater-feed system.

371 To gain insight into the process removal efficacy, the effect of both phosphate (concentration
 372 range 2 to 123 mg L⁻¹) and ammonia (concentration range 4 to 239 mg L⁻¹) initial
 373 concentration was examined, since it has been inferred that changes in the chemical
 374 composition of wastewater can affect the simultaneous recovery of both phosphate and
 375 ammonia (Muhmood et al., 2019). Results are shown in Figure 6.



376

377 **Figure 6:** Variation in percentage removal of ammonia and phosphate with varying initial
 378 concentration (conditions: room temperature, 8 g of dosage in 500 mL, 30 min of mixing, and
 379 500 rpm mixing speed).

380 As shown in Figure 6, pollutants removal was observed to decrease with an increase in their
 381 initial concentration, particularly in the case of ammonia. This is an indication that the feed's
 382 precursors chemical compounds are getting depleted with an increase in pollutant
 383 concentration, thus leading to a reduction in their removal efficiency. It should be mentioned
 384 that the system is highly efficient in removing phosphate, as shown in the corresponding Y-
 385 axis (left-hand-side) of Figure 6 (phosphate removal >99.80% for the concentration spectrum
 386 2 - 123 mg L⁻¹ and with 16 g L⁻¹ feed dosage). More specifically, when phosphate initial
 387 concentration is between 0 to 41 mg L⁻¹, the system performance is optimised, with 100 %
 388 phosphate removal. For values higher than 41 mg L⁻¹ the system's removal efficiency appears
 389 to sharply reduces, nonetheless for practical applications it remains more or less constant

390 since for 82 mg L⁻¹ initial concentration phosphate removal is 99.99 % and for the 123 mg L⁻¹
391 value phosphate removal is 99.84 %.

392 On the other hand, ammonia removal is optimised for initial ammonia concentration in the
393 range of 8 to 41 mg L⁻¹, beyond that, the removal efficiency was observed to gradually
394 decrease. Specifically, for values 8 to 40 mg L⁻¹ ammonia removal is totally reduced (100 %
395 removal), then it starts to decrease, with a sharp decrease in ammonia removal efficiency
396 being observed for values higher than 80 mg L⁻¹. In that regard, it can be inferred that 16 g L⁻¹
397 of mechano-thermo activated magnesite (feed) is sufficient to remove ≤ 123 and 80 mg L⁻¹
398 of phosphate and ammonia, respectively. Results also suggest that, as with all wastewater
399 treatment methods, the proposed method could operate as part of a treatment train, for the
400 efficient removal of both phosphate and particularly ammonia.

401 **3.2.4 Pollutants removal as a function of pH**

402 The effect of the pH on TDS, phosphate, and ammonia removal was examined by taking into
403 account a wide spectrum of pH values, ranging from as low as 1 to as high as 12 (Table 1).
404 The results for TDS are shown in Figure A6, in the appendix, where the initial and final (after
405 treatment) pH level, along with the TDS level, are shown. It was observed that for pH values
406 1 and 2 the TDS level is very low, even at contact time 0 min, and it becomes minuscule after
407 10 min treatment (Figure A6, appendix). Furthermore, for pH values in the range of 3 to 8,
408 TDS decreases with increasing pH, however, for pH values higher than 8 TDS increases with
409 increasing pH values. This could be attributed to Mg precipitation from the aqueous system,
410 hence making the system deficient of one of its main components. Nonetheless, for pH values
411 higher than 10 the system is dominated by Ca ions, thus making them the best candidate for
412 anions removal. Therefore, the treatment system was observed to be dependent on pH. The
413 pH of the final solution was also observed to increase with an increase in initial pH. The most
414 effective conditions were observed to be in the range of pH 8.5 to 10. This was also
415 corroborated by examining the pollutants percentage removal as a function of pH, while also
416 the Mg and Ca concentration/level were measured (Figure A7, appendix).

417 Specifically, in Figure A7 it is observed that pollutants percentage removal increases with
418 increasing pH in the range of 2 to 10. Thereafter, i.e. for pH values higher than 10, a large
419 reduction in phosphate removal is observed, however, ammonia removal keeps increasing
420 with increasing pH. More specifically, regarding the efficiency of the system in phosphate

421 removal, this was found to be very efficient since it was observed to be > 99% for pH values
422 in the range of 1 to 10, however, it drops drastically for pH values between 10 to 12.
423 Furthermore, the levels of Mg and Ca were also observed to decrease with an increase in pH,
424 while at pH >10 they appeared to have been depleted and this is directly proportional to the
425 level of phosphate in solution. A rapid decrease in Mg and Ca concentration was also
426 observed for pH values 2 – 3, which is proportional to the levels of TDS in the system. As
427 mentioned above the percentage of ammonia removal keeps increasing with increasing pH,
428 however the observed steep increase in ammonia removal after the value 10 probably cannot
429 be attributed to the mechano-thermo activated magnesite process per se, since pH > 10
430 promote the loss of ammonia to air due to stripping (Sutiyono et al., 2016). Therefore, pH in
431 the range 8 - 10 was observed to be suitable for the removal of both phosphate and ammonia
432 (Figure A7, appendix). Similar results were reported by Stolzenburg et al. (2015).

433 **3.2.5 Variation of pollutants removal as a function of temperature**

434 The influence of temperature on TDS and pollutants removal efficiency is examined here. As
435 detailed in Table 1, the examined temperature range is from 35 to 75 °C, while ambient pH
436 was used (7.56 to 7.79). The effect of temperature on TDS removal was first examined and it
437 is observed that TDS removal practically remains constant, regardless of temperature
438 variations (Figure A8, appendix). However, some small variations in the TDS levels were
439 observed, nonetheless these can be mainly attributed to pH changes. This suggested that TDS,
440 and, by extension pollutants removal is practically independent of the temperature. As such,
441 the results suggest that process scale-up could be conducted under South Africa's temperate
442 climate, to make this technology cost- and energy-efficient as well as environmentally
443 friendly.

444 To examine this assumption, the effect of temperature on pollutants removal was also
445 examined (Figure A9, appendix). It was observed that phosphate removal was independent of
446 temperature, nevertheless, at first glance, it appears that ammonia removal is somewhat
447 dependent on temperature, since a steep increase in ammonia percentage removal is observed
448 from the 35 °C to 45 °C and thereafter the percentage removal slightly improves with
449 increasing temperature (Figure A9, appendix). However, this is most probably attributed to
450 the fact that ammonia evaporates at temperatures higher than 30 °C, as reported by Sutiyono
451 et al. (2016), and not to the mechano-thermo activated magnesite process per se. The Mg
452 levels were observed to be dependent on temperature, as they rapidly decreased with an

453 increase in temperature, hence denoting a rapid reaction with the pollutants. This is an
454 indication that struvite formation is endothermic, because it requires additional energy for
455 optimal removal of struvite. Furthermore, the Ca levels were observed to gradually increase
456 with an increase in temperature, hence offsetting the TDS of the defined system. In light of
457 that, 55 °C appears to be the optimum temperature for pollutants, and particularly for
458 ammonia, removal. However, for industrial deployment applications and to make this
459 technology simpler to apply and energy friendly, and by extension commercially appealing,
460 the system should be scaled up under South Africa's temperate climate, rather than 55 °C
461 temperature. We should also note here that in our future works we plan to assess the
462 environmental footprint of the process, examining also the effect of additional energy and
463 ammonia emissions when the process operates at 55 °C temperature.

464

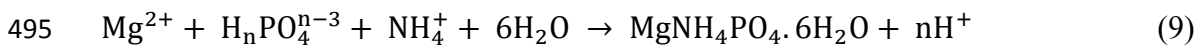
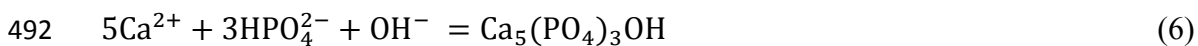
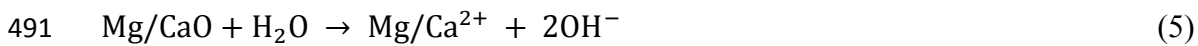
465 **4 Treatment of municipal effluents at optimised conditions**

466 Finally, the real wastewater effluent was treated under the optimum conditions, identified in
467 sections 3.2.1 – 3.2.5 (30 min and 4 g: 500 mL dosage, ambient temperature and pH). In
468 Table B1 in the appendix, the main characteristics of the raw municipal wastewater used
469 throughout this work, as well as the main characteristics of the treated effluent, under the
470 identified optimum conditions, are reported.

471 It can be inferred from Table B1 (appendix) that the optimised system can effectively remove
472 pollutants from real municipal effluents, by means of a simple and easily accessible
473 mechano-thermo treated cryptocrystalline magnesite technology. Specifically, the main
474 pollutants under study, i.e. phosphate and ammonia, were drastically reduced, particularly
475 phosphate which was practically removed. Furthermore, an increase in the pH, from 7.5 to
476 10.8, indicates that a reaction took place between the feed (mechano-thermo activated
477 magnesite) and the wastewater, leading to struvite formation. EC and TDS were also
478 observed to decrease, which further support that there is a large attenuation of pollutants from
479 the aqueous media. Specifically, sulphate was reduced from 150 to 40 mg L⁻¹; phosphate was
480 practically removed, from 120 to 0 mg L⁻¹; whereas ammonia was reduced from 135 to 30
481 mg L⁻¹, hence suggesting struvite formation (Table B1, appendix). The levels of magnesium
482 and calcium were also observed to have decreased significantly, which implies a possible co-
483 precipitation during the struvite formation.

484 **5 Mechanisms governing pollutants removal**

485 Taking into account the abovementioned results, it appears that the removal of phosphate and
486 ammonia from wastewater is mainly attributed to a combination of adsorption and
487 precipitation. Specifically, adsorption precedes precipitation and then struvite crystallization,
488 (Li et al., 2017) leading to the formation of a number of valuable substances, by the
489 mechanisms shown below. Specifically, equations (5) – (9) depict the route for the formation
490 of the final products, eventually leading to struvite formation:



496 where $n = 0, 1, 2$, etc., and it corresponds with the solution pH (Peng et al., 2018).

497 Therefore, as is suggested by equations (5) – (9) the presence of Mg and Ca will lead to the
498 effective treatment of the municipal effluents via crystallization of calcium phosphate and
499 struvite synthesis process. Similar inferences were reported by Peng et al. (2018). Finally, it
500 should be noted that this system cannot be purely defined by adsorption models, since the
501 process is not reversible and it is not utterly a surface phenomenon, hence warranting its
502 classification as a precipitation process that leads to a crystallization process.

503 **6 Conclusions**

504 Mechano-thermo treated cryptocrystalline magnesite (feed) was successfully employed for
505 the removal of phosphate and ammonia, among other pollutants, from real municipal
506 wastewater effluents. Operational parameters of the treatment process were assessed and the
507 optimised parameters were observed to vary for phosphate (5 min of mixing, 0.5 g of feed
508 dosage in 500 mL or 1 g L⁻¹, 123 mg L⁻¹ initial phosphate concentration, and pH 8 – 10) and
509 for ammonia (180 min, 16 g L⁻¹ dosage, 80 mg L⁻¹ concentration, pH 10 and > 45°C)
510 removal. The optimal conditions for the removal of both phosphate and ammonia were
511 identified to be 30 min, 3 g L⁻¹ dosage, ambient pH and temperature (7.5 pH and 35 °C
512 respectively), and 120 and 135 mg L⁻¹ initial phosphate and ammonia concentration,

513 respectively. The above suggest that the system can be part of a treatment train and/or be
514 tailored according to the initial wastewater characteristics and the targeted water quality of
515 the treated effluent.

516 Furthermore, XRD confirmed the presence of struvite in the produced sludge, hence
517 indicating that the removed pollutants react with the feed, leading to struvite formation, a
518 valuable process co-product. This was further confirmed by the FT-IR analysis, which
519 revealed the presence of N-H, Mg-O and P groups in the matrices of the product mineral
520 (sludge). Struvite can be used as a replacement of mined phosphate fertilizers and it is also
521 rich in nitrogen and magnesium, suggesting its production can valorise the wastewater
522 treatment process and promote wastewater sustainable management. Furthermore, the water
523 quality analyses revealed that the treated effluent is suitable for irrigation purposes, since
524 most of the pollutants that may trigger algal growth have been effectively removed by the
525 mechano-thermo activated magnesite driven system. Overall, with the proposed treatment
526 process not only phosphate and ammonia are effectively removed, but struvite is also
527 produced, thus leading to the valorisation of wastewater treatment process and opening new
528 horizons for the effective and sustainable management of wastewater effluents.

529 **Acknowledgments**

530 The authors of this paper would like to their profound gratitude to Tshwane University of
531 Technology, the Council for Scientific and Industrial Research (CSIR); City of Tshwane (CoT);
532 University of South Africa (UNISA); the Water Research Commission (WRC); Magalies Water
533 (MW); and National Research Foundation (NRF) for extending their support and facilities in ensuring
534 that this project is realised.

535

536 **References**

- 537 Bayuseno, A.P., Schmahl, W.W., 2018. Hydrothermal synthesis of struvite and its phase transition:
538 Impacts of pH, heating and subsequent cooling methods. *Journal of Crystal Growth* 498, 336-345.
- 539 Benyoucef, S., Amrani, M., 2012. Adsorptive removal of phosphate from aqueous solution by
540 chemically modified biosorbent. *Desalination and Water Treatment* 44, 306-313.
- 541 Chiban, M., Zerbet, M., Sinan, F., 2012. Low-cost materials for phosphate removal from aqueous
542 solutions, *Phosphates: Sources, Properties and Applications*, pp. 1-41.
- 543 Deng, H., Chen, Y., Cao, Y., Chen, W., 2016. Enhanced phosphate and fluoride removal from aqueous
544 solution by ferric-modified chromium (III)-fibrous protein. *Journal of the Taiwan Institute of
545 Chemical Engineers* 68, 323-331.
- 546 Egle, L., Rechberger, H., Krampe, J., Zessner, M., 2016. Phosphorus recovery from municipal
547 wastewater: An integrated comparative technological, environmental and economic assessment of P
548 recovery technologies. *Science of the Total Environment* 571, 522-542.
- 549 Gao, Y., Liang, B., Chen, H., Yin, P., 2018. An experimental study on the recovery of potassium (K) and
550 phosphorous (P) from synthetic urine by crystallization of magnesium potassium phosphate.
551 *Chemical Engineering Journal* 337, 19-29.
- 552 Goh, K.-H., Lim, T.-T., Dong, Z., 2008. Application of layered double hydroxides for removal of
553 oxyanions: A review. *Water Research* 42, 1343-1368.
- 554 Herald, E., Rahmawati, F., Heriyanto, Putra, D.P., 2017. Preparation of struvite from desalination
555 waste. *Journal of Environmental Chemical Engineering* 5, 1666-1675.
- 556 Huang, W., Zhang, Y., Li, D., 2017. Adsorptive removal of phosphate from water using mesoporous
557 materials: A review. *Journal of Environmental Management* 193, 470-482.
- 558 Kozik, A., Hutnik, N., Piotrowski, K., Matynia, A., 2014. Continuous reaction crystallization of struvite
559 from diluted aqueous solution of phosphate(V) ions in the presence of magnesium ions excess.
560 *Chemical Engineering Research and Design* 92, 481-490.
- 561 Li, B., Boiarkina, I., Yu, W., Huang, H.M., Munir, T., Wang, G.Q., Young, B.R., 2019. Phosphorous
562 recovery through struvite crystallization: Challenges for future design. *Science of The Total
563 Environment* 648, 1244-1256.
- 564 Li, X., Zhu, W., Wu, Y., Wang, C., Zheng, J., Xu, K., Li, J., 2015. Recovery of potassium from landfill
565 leachate concentrates using a combination of cation-exchange membrane electrolysis and
566 magnesium potassium phosphate crystallization. *Separation and Purification Technology* 144, 1-7.
- 567 Li, Z., Sun, X., Huang, L., Liu, D., Yu, L., Wu, H., Wei, D., 2017. Phosphate adsorption and precipitation
568 on calcite under calco-carbonic equilibrium condition. *Chemosphere* 183, 419-428.
- 569 Liu, X., Wang, J., 2019. Impact of calcium on struvite crystallization in the wastewater and its
570 competition with magnesium. *Chemical Engineering Journal* 378, 122121.
- 571 Magagane, N., Masindi, V., Ramakokovhu, M.M., Shongwe, M.B., Muedi, K.L., 2019. Facile thermal
572 activation of non-reactive cryptocrystalline magnesite and its application on the treatment of acid
573 mine drainage. *Journal of Environmental Management* 236, 499-509.
- 574 Masindi, V., 2017. Recovery of drinking water and valuable minerals from acid mine drainage using
575 an integration of magnesite, lime, soda ash, CO₂ and reverse osmosis treatment processes. *Journal
576 of Environmental Chemical Engineering* 5, 3136-3142.
- 577 Masindi, V., Gitari, M.W., Tutu, H., De Beer, M., 2016a. Fate of inorganic contaminants post
578 treatment of acid mine drainage by cryptocrystalline magnesite: Complimenting experimental
579 results with a geochemical model. *Journal of Environmental Chemical Engineering* 4, 4846-4856.
- 580 Masindi, V., Madzivire, G., Tekere, M., 2018a. Reclamation of water and the synthesis of gypsum and
581 limestone from acid mine drainage treatment process using a combination of pre-treated magnesite
582 nanosheets, lime, and CO₂ bubbling. *Water Resources and Industry* 20, 1-14.
- 583 Masindi, V., Ndiritu, J.G., Maree, J.P., 2018b. Fractional and step-wise recovery of chemical species
584 from acid mine drainage using calcined cryptocrystalline magnesite nano-sheets: An experimental
585 and geochemical modelling approach. *Journal of Environmental Chemical Engineering* 6, 1634-1650.

586 Masindi, V., Osman, M.S., Mbhele, R.N., Rikhotso, R., 2016b. Fate of pollutants post treatment of
587 acid mine drainage with basic oxygen furnace slag: Validation of experimental results with a
588 geochemical model. *Journal of Cleaner Production* 172, 2899-2909.

589 Mavhungu, A., Mbaya, K., Masindi, V., Muedi, K.L., Mpenyana-Monyatsi, L., 2018. Facile Synthesis of
590 Struvite from Municipal Wastewater Using Pre-Treated Magnesite, 10th Int'l Conference on
591 Advances in Chemical, Agricultural, Biological & Environmental Sciences (ACABES-18) Nov. 19-20
592 2018 Cape Town, South Africa.

593 Muhmood, A., Lu, J., Dong, R., Wu, S., 2019. Formation of struvite from agricultural wastewaters and
594 its reuse on farmlands: Status and hindrances to closing the nutrient loop. *Journal of Environmental*
595 *Management* 230, 1-13.

596 Peng, L., Dai, H., Wu, Y., Peng, Y., Lu, X., 2018. A comprehensive review of phosphorus recovery from
597 wastewater by crystallization processes. *Chemosphere* 197, 768-781.

598 Satoshi, Y., Seichiro, O., Hiroyuki, H., kotaro, A., Mitoma, Y., Hidetaka, K., Biswas, B.K., 2013.
599 Simultaneous crystallization of phosphate and potassium as magnesium potassium phosphate using
600 bubble column reactor with draught tube. *Journal of Environmental Chemical Engineering* 1, 1154-
601 1158.

602 Stolzenburg, P., Capdevielle, A., Teychené, S., Biscans, B., 2015. Struvite precipitation with MgO as a
603 precursor: Application to wastewater treatment. *Chemical Engineering Science* 133, 9-15.

604 Sutiyono, S., Edahwati, L., Perwitasari, D.S., Muryanto, S., Jamari, J., Bayuseno, A.P., 2016. Synthesis
605 and Characterisation of Struvite Family Crystals by An Aqueous Precipitation Method. *MATEC Web*
606 *of Conferences* 58, 01006.

607 Taddeo, R., Honkanen, M., Kolppo, K., Lepistö, R., 2018. Nutrient management via struvite
608 precipitation and recovery from various agroindustrial wastewaters: Process feasibility and struvite
609 quality. *Journal of Environmental Management* 212, 433-439.

610 Torzewska, A., Różalski, A., 2015. Various intensity of *Proteus mirabilis*-induced crystallization
611 resulting from the changes in the mineral composition of urine. *Acta biochimica Polonica* 62, 127-
612 132.

613 Wang, H., Wang, X., Xia, P., Song, J., Ma, R., Jing, H., Zhang, Z., Cheng, X., Zhao, J., 2017. Eco-friendly
614 synthesis of self-existed magnesium oxide supported nanorod-like palygorskite for enhanced and
615 simultaneous recovery of nutrients from simulated wastewater through adsorption and in-situ
616 struvite formation. *Applied Clay Science* 135, 418-426.

617 Wąsik, E., Bugajski, P., Chmielowski, K., Nowak, A., Mazur, R., 2017. Crystallization of struvite and
618 hydroxyapatite during removal of biogenic compounds on the filter bed. *Przemysł Chemiczny* 96,
619 1739-1743.

620 Yagi, S., Fukushi, K., 2012. Removal of phosphate from solution by adsorption and precipitation of
621 calcium phosphate onto monohydrocalcite. *Journal of Colloid and Interface Science* 384, 128-136.

622 Yan, H., Shih, K., 2016. Effects of calcium and ferric ions on struvite precipitation: A new assessment
623 based on quantitative X-ray diffraction analysis. *Water Research* 95, 310-318.

624 Zulfiqar, M., Omar, A.A., Chowdhury, S., 2014. Removal of phosphate and fluoride from industrial
625 wastewater – A short review, *Applied Mechanics and Materials*, pp. 805-808.

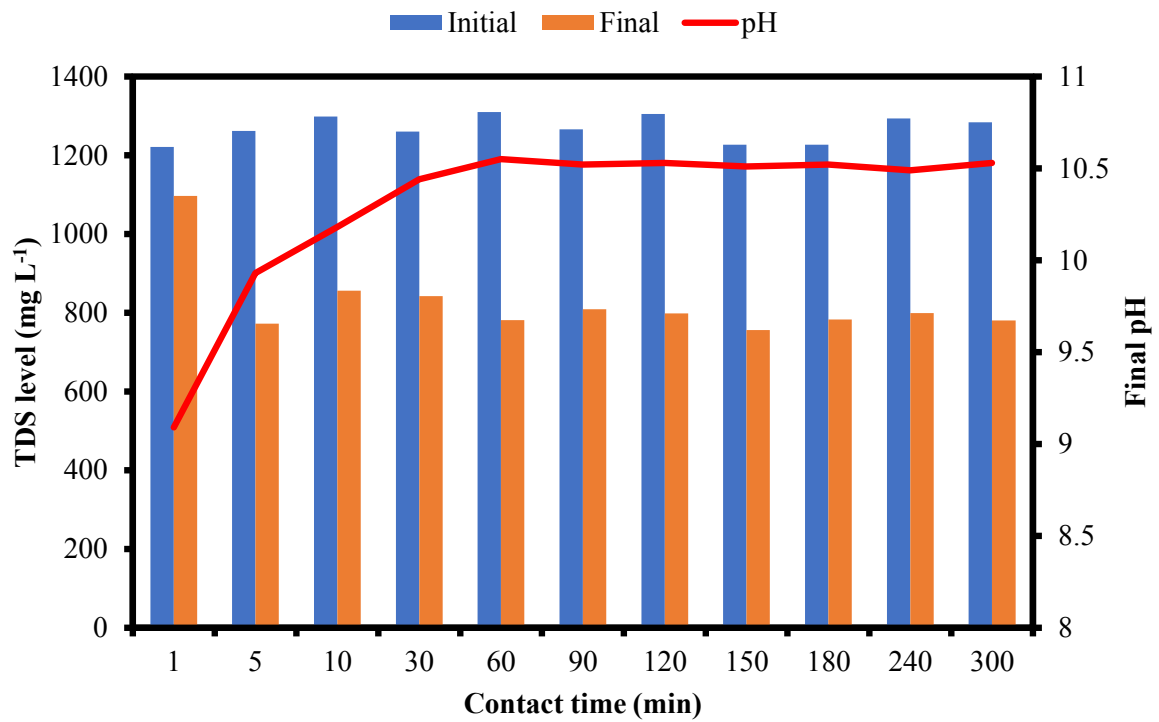
626

627

628 **Appendix A – Operational parameters optimisation figures**

629

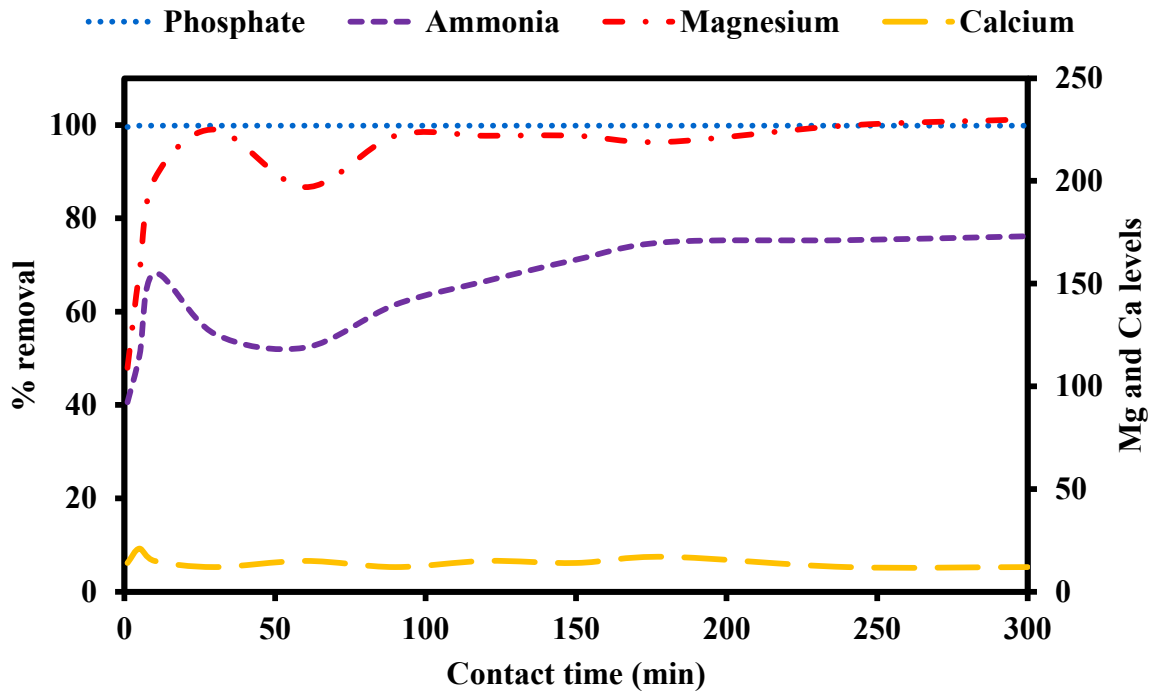
630



631

632 **Figure A1:** Variation in TDS with an increase in contact time (conditions: 1 g: 100 mL S/L
633 ratios, room temperature, 1 g of pre-treated magnesite and 500 rpm mixing speed).

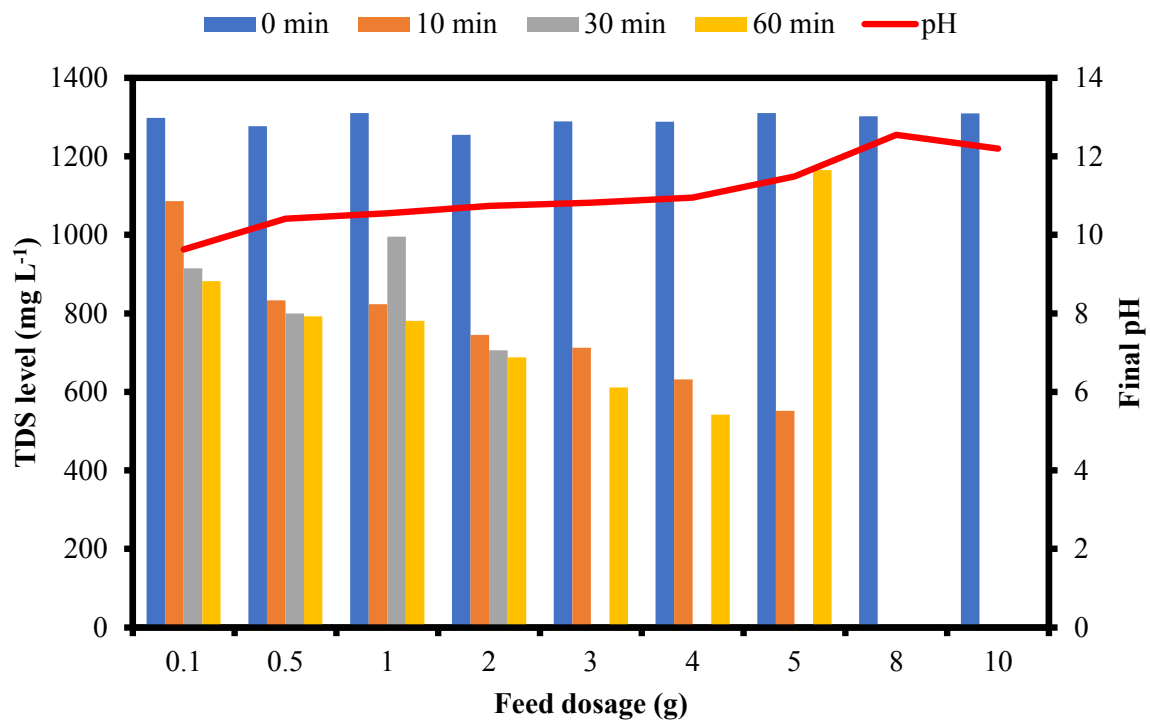
634



635

636 **Figure A2:** The variation in percentage removal of ammonia and phosphate along with the
 637 levels of calcium and magnesium, with varying contact time (conditions: 1 g: 100 mL S/L
 638 ratios, room temperature, 1 g of pre-treated magnesite, and 500 rpm mixing speed).

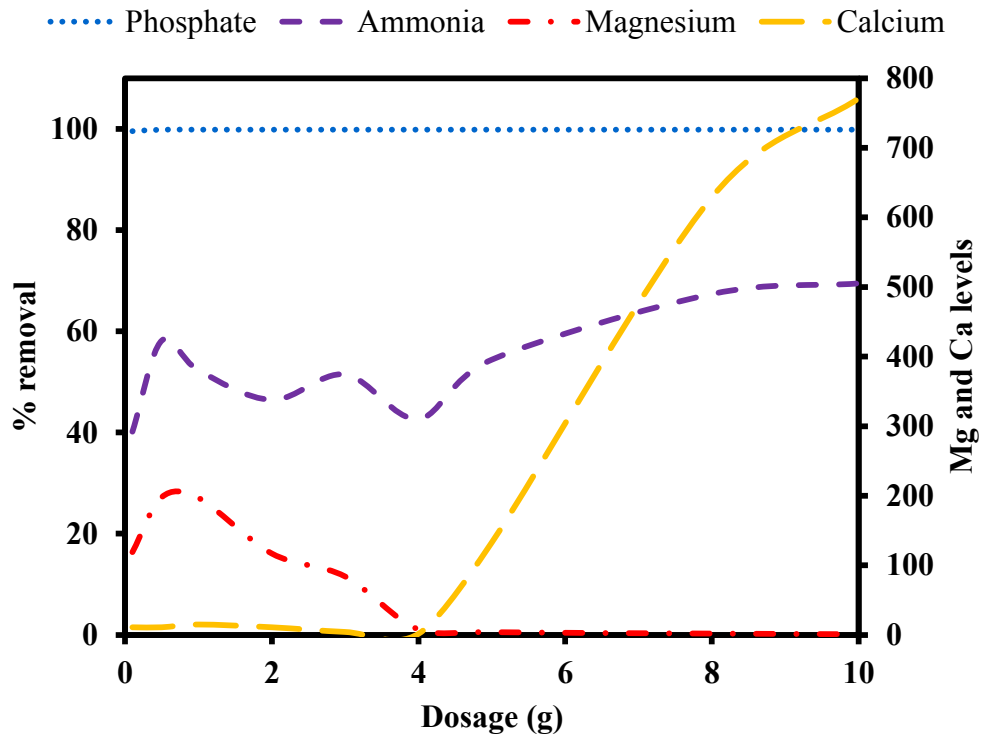
639



640

641 **Figure A3:** Variation in TDS concentration with increasing feed dosage and contact time
 642 (conditions: room temperature, pH > 6.5, 500 rpm mixing speed, time : 10 to 60 min, 123
 643 ppm for phosphate, 80 ppm for ammonia, and room temperature)

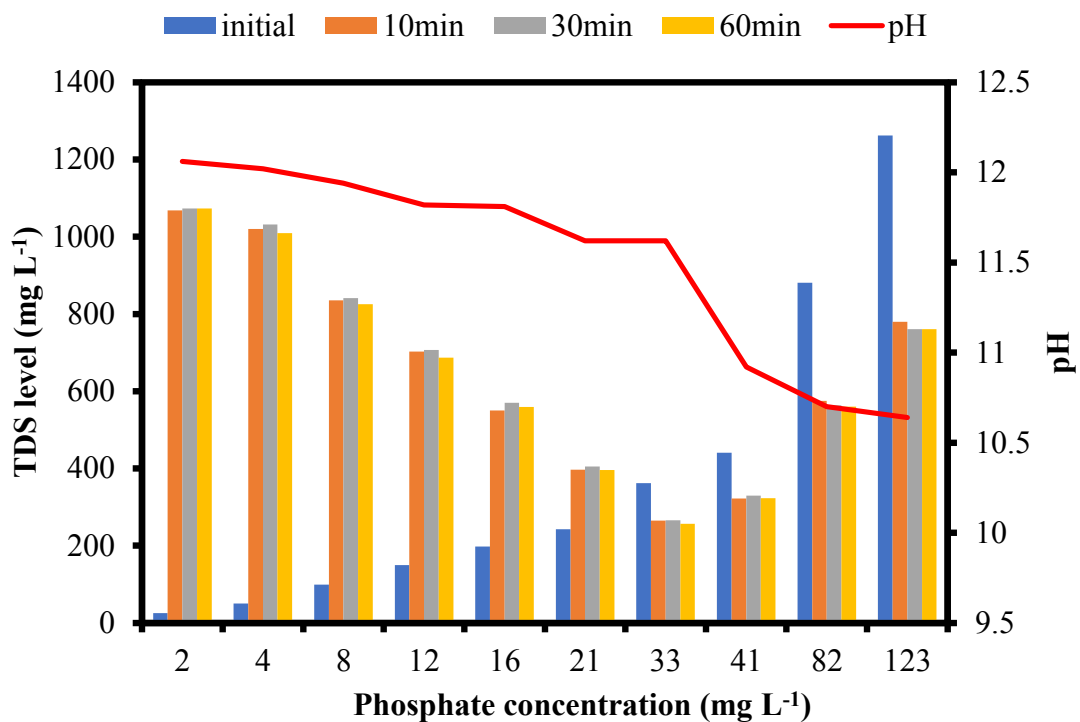
644



645

646 **Figure A4:** Variation in percentage removal of ammonia and phosphate, along with the
 647 levels of calcium and magnesium, with varying feed dosage (conditions: 500 mL volume,
 648 room temperature, contact time 30 min and 500 rpm mixing speed).

649

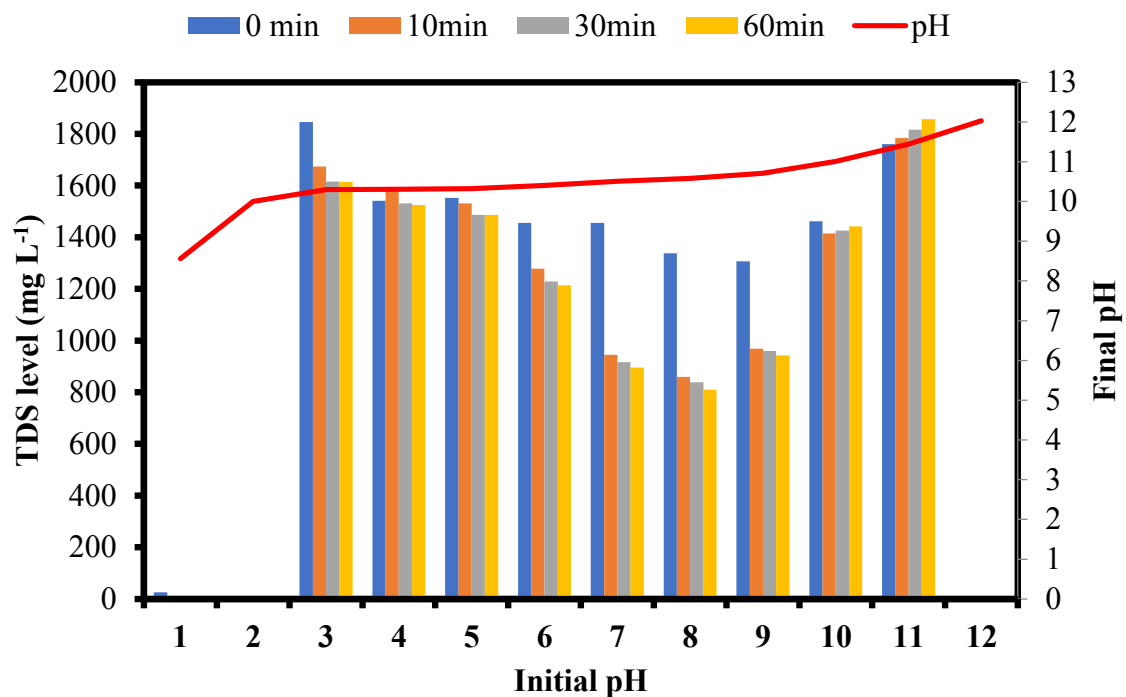


650

651 **Figure A5:** Variation in TDS with a variation in phosphate initial concentration (conditions:
 652 room temperature, 30 min of mixing, pH > 6.5, 8 g: 500 mL, and 500 rpm mixing speed).

653

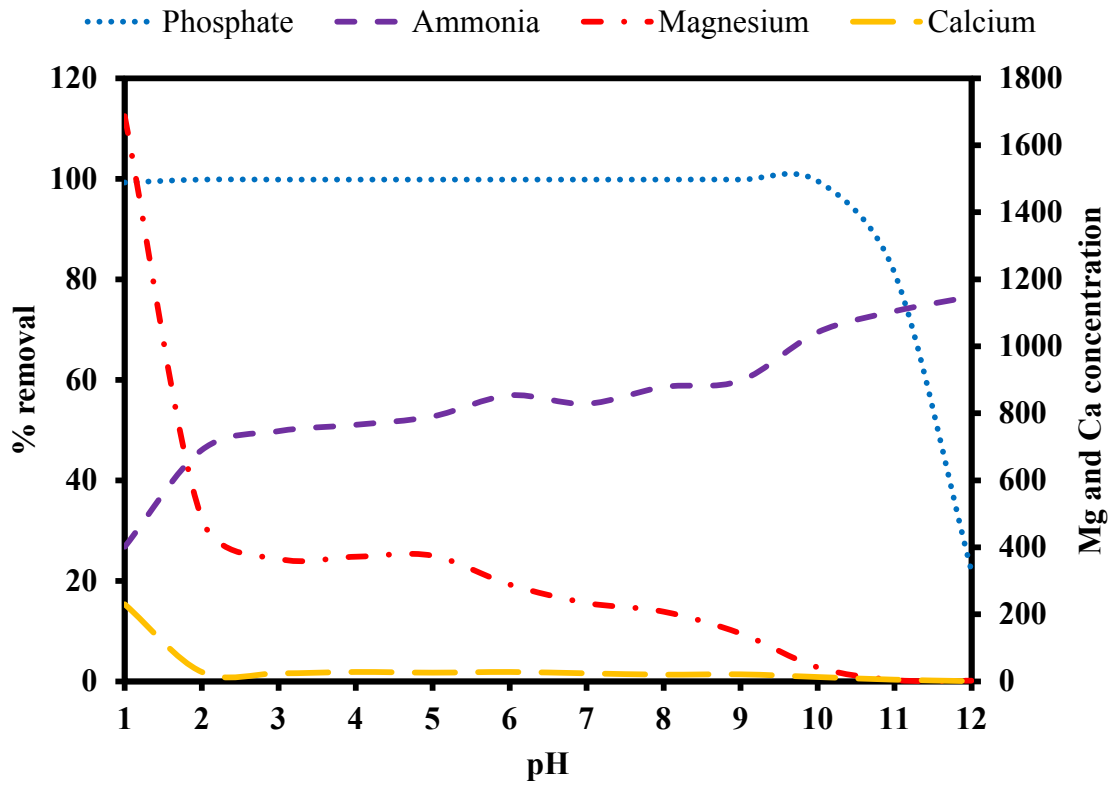
654



655

656 **Figure A6:** Influence of the initial pH level on TDS removal and on the final pH level
 657 (conditions: room temperature, feed dosage 8 g: 500 mL, 500 rpm mixing speed, 123 ppm for
 658 phosphate, and 80 ppm for ammonia).

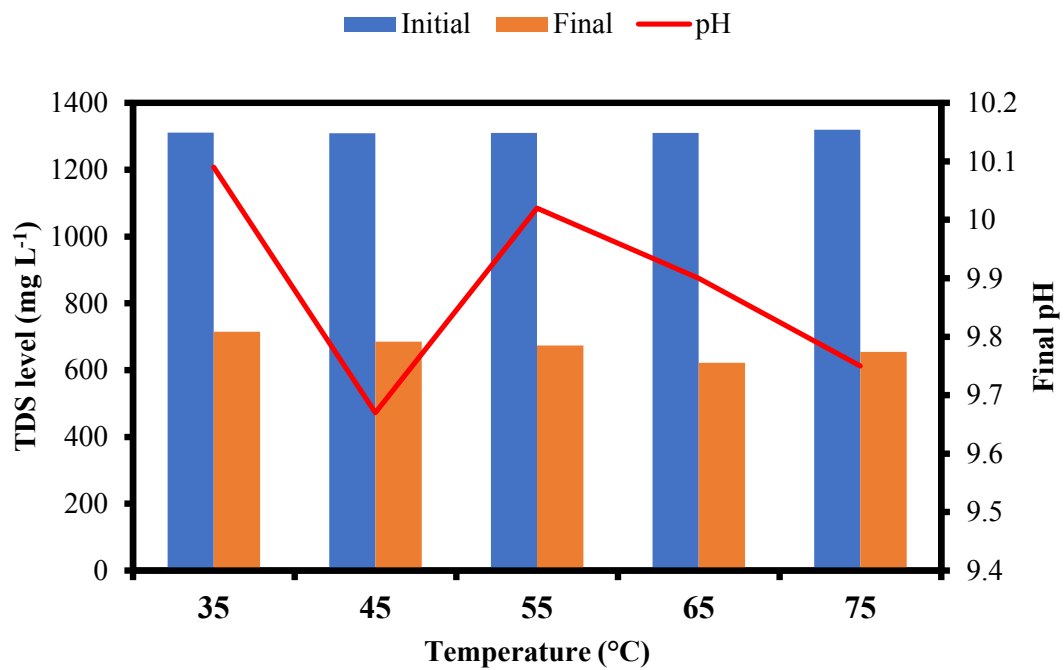
659



660

661 **Figure A7:** Variation in percentage removal of ammonia and phosphate with varying pH and
 662 influence on Mg and Ca concentration (conditions: room temperature, 30 min contact time, 8
 663 g : 500 mL of dosage, ≤ 123 and 80 mg/L of phosphate and ammonia, and 500 rpm mixing
 664 speed).

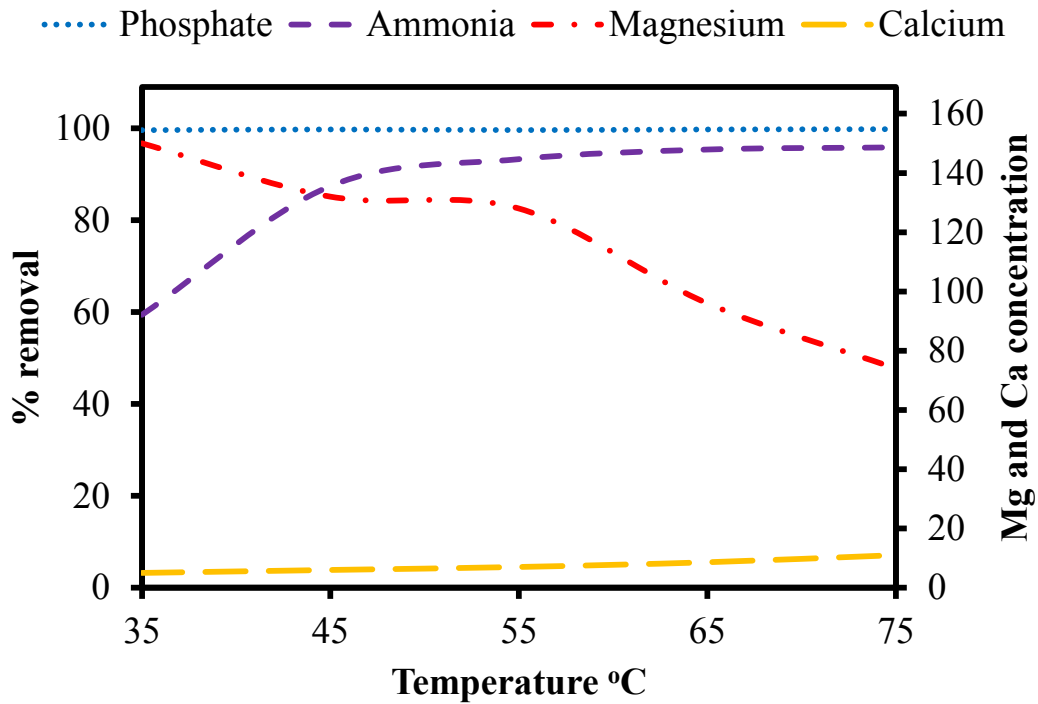
665



666

667 **Figure A8:** Influence of temperature on TDS removal (conditions: 30 min, 8 g: 500 mL, 500
 668 rpm mixing speed, 123 ppm for phosphate, and 80 ppm for ammonia, pH between 7.56 to
 669 7.79).

670



671

672 **Figure A9:** Variation in percentage removal of phosphate and ammonia under different
 673 temperature gradients (conditions: 30 min, room temperature, 4 g: 500 mL of dosage, ≤ 123
 674 and 80 mg/L of phosphate and ammonia, and 500 rpm mixing speed).

675

676

677

678 **Appendix B – Raw wastewater and treated effluent characteristics**

679 **Table B1:** Main characteristics of the raw wastewater and the treated effluent under optimal
 680 conditions, i.e. 30 min and 4 g: 500 mL dosage.

Parameters	Units	Raw municipal effluents	Treated effluent
Aluminium	mg L ⁻¹	<0.00073	<0.00073
Ammoniacal Nitrogen	mg L ⁻¹	135	30
Antimony	mg L ⁻¹	0.0017	0.0011
Arsenic	mg L ⁻¹	0.0035	0.0034
Barium	mg L ⁻¹	0.011	0.0058
Boron	mg L ⁻¹	<0.16	<0.16
Cadmium	mg L ⁻¹	<0.0002	<0.0002
Calcium	mg L ⁻¹	200	0.2
Chloride	mg L ⁻¹	76	81
Chlorine (free)	mg L ⁻¹	0.07	0.04
Chromium	mg L ⁻¹	0.00037	0.0013
Colour	mg L ⁻¹	44	33
Copper	mg L ⁻¹	0.0013	0.0007
Cyanide total	mg L ⁻¹	<0.010	<0.010
Electrical conductivity (EC)	mS/cm	200	120
Flouride	mg L ⁻¹	<0.2	1.2
Iron	mg L ⁻¹	0.015	<0.00088
Lead	mg L ⁻¹	<0.00011	<0.00011
Magnesium	mg L ⁻¹	1600	0.5
Manganese	mg L ⁻¹	0.022	<0.00025
Mercury	mg L ⁻¹	<0.00045	<0.00045
Monochloramine	mg L ⁻¹	0.03	<0.010
Nickel	mg L ⁻¹	0.017	0.013
Nitrate + Nitrite	mg L ⁻¹	1.5	1.3
Nitrate Nitrogen	mg L ⁻¹	1.4	1.3
Nitrite Nitrogen	mg L ⁻¹	<0.2	<0.2
pH	N/A	7.5	10.82
Phenols	mg L ⁻¹	<0.01	<0.01
Phosphate	mg L ⁻¹	120	<0.001
Selenium	mg L ⁻¹	<0.0021	<0.0021
Sodium	mg L ⁻¹	77	74
Sulphate	mg L ⁻¹	150	40
TDS	mg L ⁻¹	2900	756
Turbidity	NTU	10	2.9
Uranium	mg L ⁻¹	<0.00008	<0.00008
Zinc	mg L ⁻¹	0.014	<0.00057